

Long-lived volcanic resurfacing of Venus driven by early collisions

Received: 16 April 2023

Accepted: 20 June 2023

Published online: 20 July 2023

 Check for updates

Simone Marchi¹✉, Raluca Rufu^{1,2} & Jun Korenaga³

The geodynamics of Earth and Venus operate in strikingly distinct ways, in spite of their similar size and bulk density, resulting in Venus's absence of plate tectonics and young surface age (0.2–1 billion years). Venus's geophysical models have sought to explain these observations by invoking either stagnant lid tectonics and protracted volcanic resurfacing, or by a late episode of catastrophic mantle overturn. These scenarios, however, are sensitive to poorly understood internal initial conditions and rheological properties, and their ability to explain Venus's young surface age remains unclear. Here we show that long-lived volcanism, driven by early, energetic collisions on Venus, offers an explanation of its young surface age with stagnant lid tectonics. This volcanic activity is fuelled by a superheated core, resulting in vigorous internal melting regardless of initial conditions. Furthermore, we find that energetic impacts stir Venus's core, suggesting that its low magnetic field is not likely to be caused by a compositionally stratified core, as previously proposed.

Terrestrial planet formation models (for example, refs. 1,2) indicate that Earth and Venus grew primarily from adjacent feeding zones with similar accretion histories. The difference in heliocentric distance between Earth and Venus could have resulted in distinct phases of giant impacts, but the number and outcome of these events are model dependent³ (Methods).

Regardless of the specific accretion histories of Earth and Venus, *N*-body simulations show that their tail-end accretions (hereinafter, late accretion) were characterized by significantly different mean impact velocities of $\approx 19 \text{ km s}^{-1}$ and $\approx 24 \text{ km s}^{-1}$ for Earth and Venus, respectively⁴. In addition, about 9% and 25% of all impacts for Earth and Venus, respectively, occurred at a velocity greater than 30 km s^{-1} (Supplementary Fig. 1). These differences arise because Venus has a shorter semimajor axis (greater orbital velocity) than Earth, and because late accretion is typically dominated by impactors originating from beyond Earth's orbit that require higher orbital eccentricities to collide with Venus than to collide with Earth.

Consequences of high-energy late-accretion collisions on Venus

Earth's late accretion was punctuated by large collisions, possibly up to $\approx 4,000 \text{ km}$ in diameter or 0.02 Earth masses, M_e (refs. 4–6).

A similar evolution is inferred for Mars⁷ and Venus⁸. Here we explore the consequences of large, high-velocity impacts on Venus. We use high-resolution smoothed-particle hydrodynamic (SPH) simulations and consider impact velocities from 19 to 30 km s^{-1} ; impact angles 0° , 30° , 45° and 60° (0° is head-on); and impactor mass $M/M_e = 0.01$, 0.003 and 0.001 (impactor diameters are 3,000, 2,000 and 1,400 km, respectively). All the projectiles are differentiated with a core to total mass ratio of 30% (Methods). We consider two internal structures for Venus, with a core to planet mass ratio of 24% and 30% (Methods), and find that they do not substantially affect the results. The initial temperature distribution is chosen to be below the solidus⁹, that is, post primordial magma ocean solidification. For comparison, we run a similar set of impact simulations for Earth (Methods).

We first quantify the amount of mantle melting, using two different methods. In the first method, we compare the change in specific entropy (ΔS) for each SPH particle¹⁰. We assume that silicate particles with $\Delta S \geq 500 \text{ J K}^{-1} \text{ kg}^{-1}$ are molten. In the second method, particles are assumed molten if the postimpact temperature of silicate particles exceeds the local temperature corresponding to 40% melting (for the same depth; Methods). The two methods give results for both Earth and Venus within 5%, which is adequate for our purposes.

¹Southwest Research Institute, Boulder, CO, USA. ²Sagan Fellow, Boulder, CO, USA. ³Yale University, New Haven, CT, USA.

✉e-mail: marchi@boulder.swri.edu

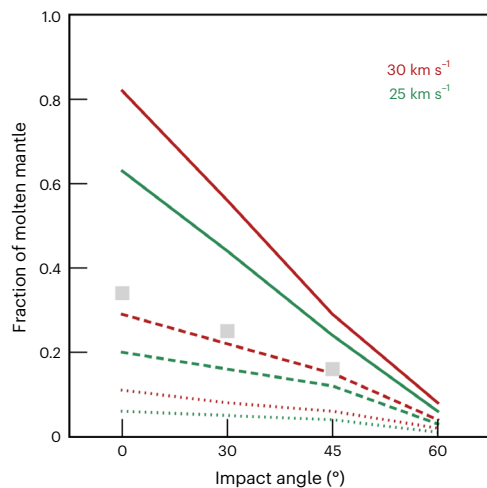


Fig. 1 | Impact-generated melt on Venus. Fraction of molten mantle for 0.01, 0.003 and 0.001 M_e projectiles (solid, dashed and dotted lines, respectively) versus impact angle, and two impact velocities (25 km s^{-1} is the average late accretion velocity for Venus, green curves). An extreme case for 30 km s^{-1} is also reported (red curves; see text). For comparison, grey squares indicate Earth's mantle melting for 0.01- M_e impactors at 19 km s^{-1} (average impact velocity for Earth).

As expected, a greater impact velocity produces more silicate melting, and for a head-on impact with 0.01 M_e at 30 km s^{-1} , about 82% of Venus's mantle is molten (Fig. 1). For terrestrial impacts with similar size and impact angle, but with the mean impact velocity of 19 km s^{-1} , the resulting fraction of molten mantle is $\approx 35\%$. We also find that the impact angle has a significant effect on melt volume¹⁰. For a collision on Venus with 0.01 M_e , at 30 km s^{-1} and at a 45° angle, the melt fraction is $\approx 30\%$, thus a drop by a factor of 2.7 compared with the head-on case. A consequence of the high impact velocity is that Venus's mantle is largely mixed (Fig. 2), and the molten material is redistributed globally in a shallow magma ocean even in the case of a low impact angle, which typically results in more localized effects at lower impact velocities (Fig. 2b and Supplementary Fig. 2a). A higher impact velocity also results in a deeper deposition into the target of the projectile kinetic energy, and an increased heating of the core.

Venus's superheated core and long-term geophysical evolution

The fact that late impacts on Venus had significantly higher velocity than those on Earth suggests that a few large impacts could have had drastically different outcomes, with important implications for the subsequent geophysical evolution.

For this, we look at the postimpact internal temperature distribution. High-energy late-accretion collisions invariably result in a peculiar thermal structure within Venus, characterized by a shallow magma ocean and a superheated core (Fig. 3 and Supplementary Figs. 2 and 3); this is a new kind of a postimpact thermal structure unavailable in studies based on simplified analytical scaling relationship (for example, refs. 8, 11, 12). The temperature increase in the core is due to a combination of the passing shock wave and the localized drop in pressure due to large-scale mantle disruption (Supplementary Fig. 4). The shallow magma ocean (600 km deep) would rapidly cool down with a time scale shorter than 10^6 years, even in the presence of a thick CO_2 -rich atmosphere^{13,14}. The superheated core, however, would more slowly dissipate heat because of the overlying insulating mantle. To address the influence of a superheated core on the long-term thermal evolution of Venus, we ran a series of parameterized convection models. Our modelling is based largely on a previous formulation¹⁵, with modifications

to handle the effect of a superheated core, the possibility of crustal delamination and the melting of mantle plumes (Methods).

The results from representative simulations, with and without high-velocity impacts, are shown in Fig. 4. In all cases, we assume a stagnant lid convection throughout the history of Venus, starting with a core potential temperature of 4,000 K and a mantle potential temperature of 1,900 K (Fig. 4a). Although the mode of mantle convection for Venus has been debated, especially for its early evolutionary phase¹⁶, stagnant lid convection is the most natural style of mantle convection with the strongly temperature-dependent viscosity of silicate rocks¹⁷. Because of its proximity to the Sun, Venus can quickly lose initial surface water, if any, by the runaway greenhouse effect^{18,19}, and the lack of surface water precludes the activation of secondary weakening mechanisms that are thought to be responsible for the operation of plate tectonics on Earth²⁰. In the reference case without a late impact, both the mantle and the core gradually cool down, and the total rate of extrusive magmatism becomes lower than $1 \text{ km}^3 \text{ yr}^{-1}$ by 1.3 billion years ago (Ga) (Fig. 4b,c). With a late accretion, here using the result for an impact with 0.01 M_e at 25 km s^{-1} and at 30° or 45° (assumed to occur 0.3 Gyr after formation), the shallow part of the core was heated almost instantly to $\approx 5,000$ – $6,000$ K on global average (Fig. 4a and Supplementary Fig. 5). It takes about a hundred million years to have a thermally homogenized core hotter than the reference case by ≈ 400 – 800 K, and this excess heat drastically alters the subsequent thermal evolution (Fig. 4a,b) by enhancing both distributed melting by small-scale convection and focused melting by mantle plumes (Fig. 4c). In particular, sublithospheric convection can sustain globally distributed extrusive magmatism at a rate exceeding $1 \text{ km}^3 \text{ yr}^{-1}$ until ≈ 400 – 800 million years ago (Ma) (Fig. 4c). An increase in mantle temperature is limited (Fig. 4a), but such an increase is sufficient to encourage lithospheric delamination to make more room for the melting of sublithospheric mantle, and heat flux from the superheated core helps to maintain this situation. The prolonged magmatism following late accretion is also consistent with the abundance of ^{40}Ar in the atmosphere within observational uncertainties¹⁵ (Fig. 4d), but we warn that the absolute values of the predicted eruption rates depend on the parameterization of mantle rheology and melting. A more robust conclusion is the increase in magmatic activity by a factor of several resulting from a late collision close to the more likely impact conditions (25 km s^{-1} , 30–45°). There is a trade-off among impact parameters, and for the same projectile mass, lower impact angles or higher impact velocities produce more volcanisms, with the extreme case (0.01 M_e , at 30 km s^{-1} and an impact angle of 0°) resulting in too extensive volcanism to be consistent with the atmospheric ^{40}Ar abundance (Supplementary Fig. 6). Note that our reference terrestrial impact (0.01 M_e , at 19 km s^{-1} and 45°) results in substantially less core heating, and thus is not capable of sustaining long-lived volcanism as discussed above for Venus (Supplementary Figs. 2 and 3). In addition, plate tectonics on Earth efficiently dissipates internal heat and reduces volcanism.

Comparison with Venus's observational constraints

This process provides a new explanation for why Venus's surface age is younger than 1 Ga. For the representative cases shown, the overall melt eruption rate drops to $1 \text{ km}^3 \text{ yr}^{-1}$ at ≈ 400 – 800 Ma. This eruption rate produces the required melt volume for global resurfacing in 100 Myr ($\approx 10^8 \text{ km}^3$) (ref. 21). As upwelling is localized in both small-scale convection and plumes, we expect that, at the lower end of the melt eruption, volcanism will be limited to localized spots. Observations of volcanically embayed craters²² suggest widespread localized volcanic eruptions covering at least 40% of surface area since the last global resurfacing²³. For the collisions reported in Fig. 4, such surface area coverage is achieved backward in a time about 100–200 Ma. Complete surface reset is achieved about 200–500 Ma. This result is compatible with a revised surface cratering age of ≈ 180 – 240 Ma

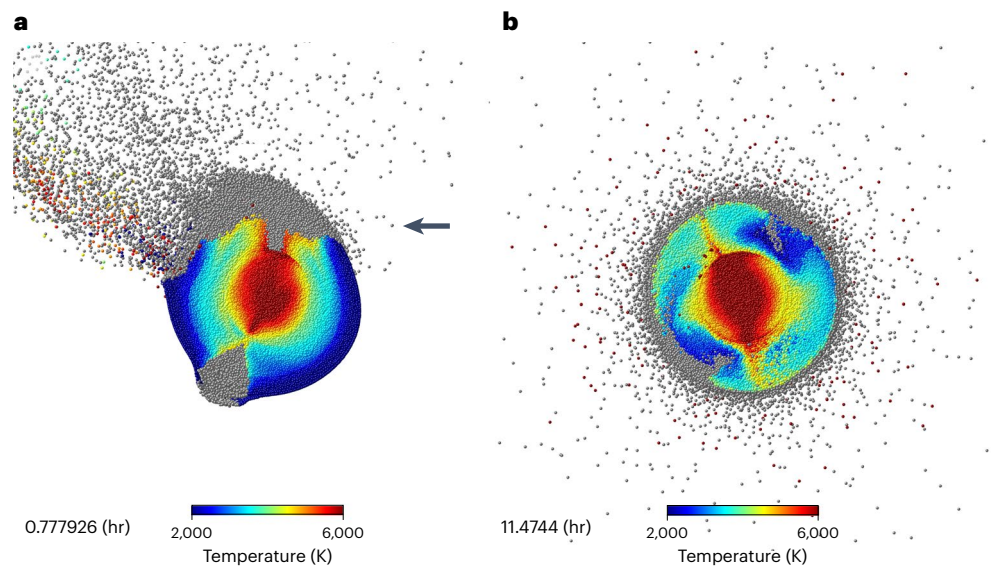


Fig. 2 | Venus's thermal evolution from an energetic collision. A simulation of a $0.01-M_{\oplus}$ projectile colliding with Venus at 25 km s^{-1} , at 45° . Grey indicates molten silicate particles. **a**, Venus at about 0.77 hours after impact. Black arrow

indicates projectile direction. Note a large molten clump at the antipode of the impact point due to pressure wave convergence. **b**, Venus at about 11.47 hours after impact.

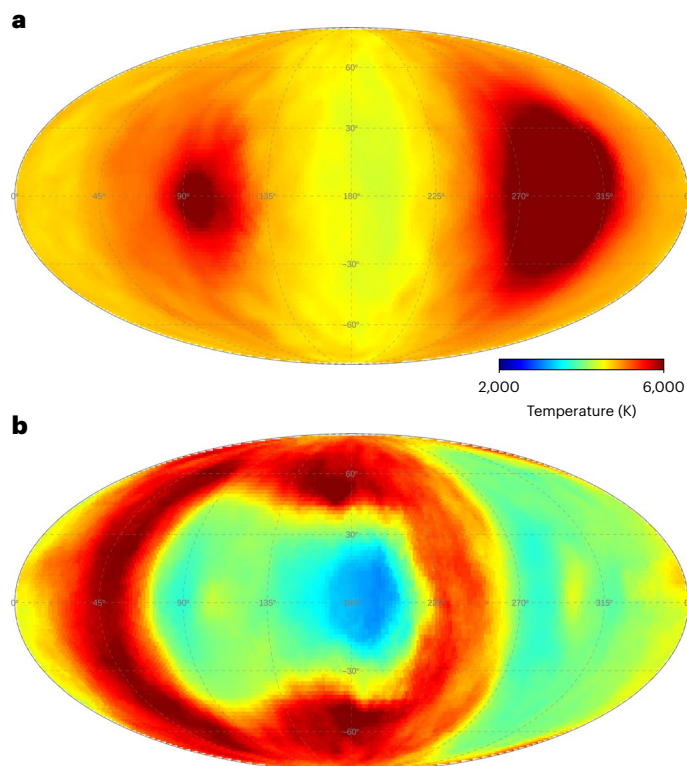


Fig. 3 | Mollweide projection of Venus's postimpact temperature. Simulation and time step as in Fig. 2b. **a**, Core radial averaged temperature for 0.45–0.47 of Venus's radius (R_v). The averaged pre-impact temperature in this spherical shell was about 4,000 K. When modelling long-term evolution, these extreme lateral variations are averaged out in parameterized convection, thereby reducing the intensity of plume magmatism in the model. **b**, Mantle radial averaged temperature for 0.98–1.00 R_v . The averaged pre-impact temperature in this spherical shell was about 1,500 K. Note the temperature in this shell is in excess of 2,000 K—thus higher than the local 40% melt temperature (Supplementary Fig. 3a)—resulting in a global magma ocean.

(refs. 24–26). Note that the reference model without energetic impacts is not compatible with these observations because of the much lower eruption rate.

Our explanation of Venus's young surface age is consistent with rock mechanics, because a common explanation invoking episodic plate tectonics^{9,27,28} requires an unrealistically low-yield stress for the lithosphere despite the lack of surface water on Venus²⁰. In addition, the ability of previous stagnant lid models without late energetic collisions (for example, refs. 9,15,29) to generate a young surface age depends on the specific combination of initial conditions (such as an initially high core or mantle temperature) and model settings (parameterization of mantle melting and volcanic eruption, as well as assumed mantle rheology), which is difficult to validate. A similar conclusion applies to alternative models invoking a late episode of catastrophic mantle overturn^{30,31}.

In our solution, energetic late accretion on Venus resets the early core to a very high temperature, regardless of its initial state, and the lack of plate tectonics helps to sustain volcanism for billions of years. Previous models¹¹ also concluded that collisions affect the long-term evolution of Venus, but only under special circumstances (for example, timing of impact). This conclusion is based on a treatment that neglects a superheated core and global magma ocean, and our results are not sensitive to timing of impact (Methods).

It has been suggested that the lack of the present-day magnetic field on Venus may be due to a chemically stratified core³². Our simulation results, however, indicate that late accretion (and, by extension, impacts during the main accretion phase) can substantially homogenize a pre-existing chemical stratification by mechanical mixing (Supplementary Fig. 7). Having only $\approx 80\%$ of Earth's mass, the internal pressure of Venus is too low to nucleate an inner core if the core composition is similar to that of Earth's core³³. Even without a chemical stratification, therefore, the lack of a current magnetic field can be explained by a low core heat flux that is not sufficient to drive a purely thermally driven dynamo (Fig. 4b). Late accretion does result in a prolonged period of high core heat flux in the past (Fig. 4b), but the resulting crustal magnetization would not be preserved to the present because of continuous magmatism (Fig. 4c), a scenario that could be tested by future magnetometer measurements³⁴.

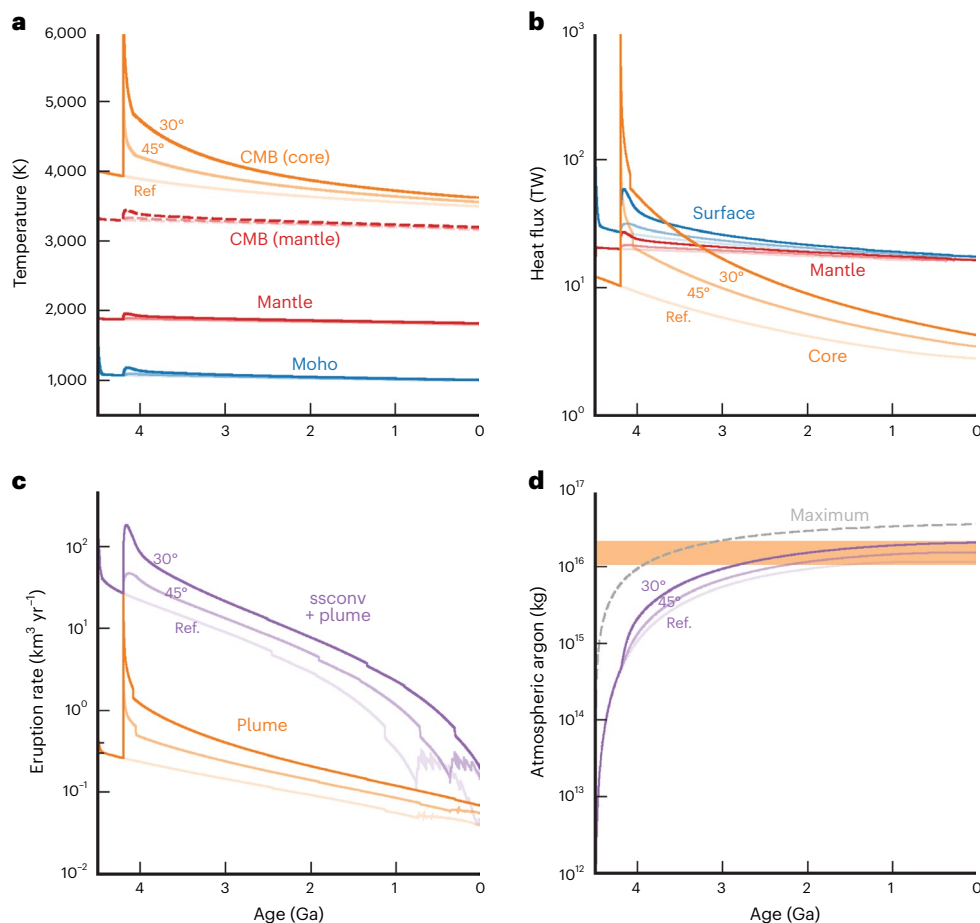


Fig. 4 | Venus's thermal evolution modelling with and without an energetic collision. Representative core–mantle simulations. **a**, Core-side core–mantle boundary (CMB) temperature (orange), mantle-side CMB temperature (red dashed), mantle potential temperature (red) and Moho temperature (blue). The reference case (Ref.) without late accretion is shown in the lightest shade. The case with an impact angle of 45° is shown in the medium shade, and the case with 30° is in the

dark shade. **b**, Core heat flux (orange), mantle heat flux (red) and surface heat flux (blue). **c**, Melt eruption rate by plume magmatism (orange), and the total eruption rate including magmatism by small-scale convection (ssconv, purple). **d**, Abundance of atmospheric ^{40}Ar released by magmatism (purple). Grey dashed line shows total ^{40}Ar abundance in Venus, and orange bar denotes the present-day atmospheric abundance⁸⁶. See Methods for details of the model set-up.

Methods

Impact simulations and Venus's accretion

We performed SPH simulations using GADGET2 (ref. 35) with a tabulated M-ANEOS equation of state (EOS) for forsterite to represent the mantle³⁶ and ANEOS for iron to represent the core³⁷. The code modifications were performed in refs. 38,39, and are available in the supplemental material of ref. 40. SPH mimics material as spherically symmetric particles, whereby the spatial distribution of each particle is defined by a spline density weighting function, called the kernel, and a characteristic radius, called the smoothing length. The kinematic state of each particle is evolved as a result of gravity, compressional heating/expansional cooling and shock dissipation; material strength is ignored (the latter approximation is adequate given the high internal pressures). The EOS accounts for phase changes and includes different phases within an SPH particle, assuming thermal equilibrium.

Venus is resolved by $\approx 8 \times 10^5$ particles and we assume a core to planet mass ratio of 24% and 30% (R. Ghail, 24 November 2020, personal communication). We assume the impactors (0.01, 0.003 and 0.001 M_{\oplus}) are differentiated with a bulk chondritic composition, core mass fraction of 30% (ref. 6). We run similar simulations for the Earth, resolved by $\approx 10^6$ particles and a 32% core to planetary mass fraction. We let the initial SPH particles relax to the hydrostatic equilibrium before impact. The temperature of the particles is adjusted and relaxed again if large deviations from the adopted initial thermal profile occur.

The temperature is calculated using the EOS table given the density and entropy output from the SPH code. SPH has difficulty in resolving sharp density discontinuities such as the core–mantle boundary^{41,42}; to ensure that the temperature changes recorded at the core–mantle boundary are not numerical artefacts, we calculated the temperature using the postimpact entropy and the pre-impact densities and compared them with the previous temperatures. The temperatures are similar within 120 K (compared with $\approx 1,500$ -K temperature change at the core–mantle boundary); hence we conclude that the temperature increase in the core is mainly due to the increase in entropy (which is an independent variable), and not the changes in density. The increase in entropy is due to unloading of the mantle during the impact and shock heating (Supplementary Fig. 4).

The primary accretion phase of Earth ended with a giant impact that resulted in the formation of the Moon (for example, ref. 43). The lack of a moon for Venus has been interpreted as a lack of a giant impact³², but SPH impact simulations indicate that large collisions could have occurred without forming moons⁴⁴. Alternatively, a moon could have been lost because of a subsequent impact that reversed the planetary spin, and the direction of the moon's tidal evolution⁴⁵.

Venus's current spin state (retrograde with a 243-d period) can result from a combination of internal and atmospheric tides, core–mantle friction and planetary perturbations^{46–49}. For a planetary tidal

dissipation factor, Q , of $Q \approx 20$ (similar to the current Earth), Venus's current spin state can be achieved in less than 4.5 Gyr, if Venus's rotation was higher than about 48 hr at the end of the late accretion⁴⁹. Most of the postimpact rotation in this suite of simulations (75%) resulted in rotations larger than 48 hr (assuming a Venusian total moment of inertia of 0.33), consistent with the expected long-term evolution of Venus's spin⁴⁹. In our impact simulations, the maximum postimpact rotation is ≈ 24 hr, which resulted from a $0.01 M_e$ impactor with a 30° impact angle at the highest impact velocity, 30 km s^{-1} . This postimpact rotation could be reconciled if Venus's tidal dissipation was larger ($Q \approx$ a few; for example, refs. 50,51) allowing for an initial Venus day as short as ≈ 12 hr.

The resulting circumplanetary debris disks are small. Adopting the scaling laws from ref. 52, we find that the accreted moons around Venus are $< 0.01 M_m$ (where M_m is the current lunar mass). If such a moon is indeed created, the subsequent tidal evolution around a slow-rotating planet will drive the moon inward⁵³. Hence, we do not expect these impacts to create long-lasting moons around Venus.

Long-term core–mantle evolution modelling

The thermal evolution of Venus in the mode of stagnant lid convection with or without a late-accretion event is modelled using the parameterization developed in refs. 15,54,55, with some modifications as described below. To be self-contained, the basic features of the original parameterization are summarized first. The model is based on the energy balances for the core, the mantle and the crust. The thermal evolution of the core is controlled by energy input from inner core nucleation (if any) and energy output by heat flux at the core–mantle boundary. The thermal evolution of the mantle is controlled by energy input from core heat flux and radiogenic heating and energy output by heat flux at the base of the crust (Moho). The melting of the mantle by small-scale convection and mantle plumes results in the formation of the crust and its growth. Heat-producing elements in the mantle are preferentially partitioned to the crust through the partial melting of the mantle, and the crustal thermal profile is calculated by taking into account radiogenic heat production within the crust and the heat flow from the mantle at the Moho. The difference between the crust-side temperature at the Moho and the potential temperature of the mantle is what drives sublithospheric convection, so the Moho temperature is calculated self-consistently with the mantle heat flux, which is in turn controlled by mantle viscosity, lithospheric viscosity and lithospheric compositional buoyancy. Surface heat flow is then calculated from the crustal thermal profile. For the upper mantle reference viscosity, we use 10^{19} Pa s at the reference potential temperature of 1,573 K and the activation energy of 300 kJ mol^{-1} . Viscosity increase by dehydration stiffening is set to 10, and the density reduction by chemical depletion is to 120 kg m^{-3} . The viscosity of Earth's upper mantle (or asthenosphere) has been estimated to be in the range of 10^{18} – 10^{19} Pa s based on the scaling of small-scale convection (for example, refs. 56,57) and in the range of 10^{19} – 10^{20} Pa s based on seamount loading and postglacial rebound (for example, refs. 58,59), and an intermediate value of 10^{19} Pa s is chosen as reference. Varying this reference viscosity, however, does not affect our conclusion that late accretion results in long-lived enhanced volcanism (Supplementary Fig. 8).

The core heat flux parameterization of ref. 15 adopts that of ref. 33, which is equivalent to using a mantle viscosity of $\approx 5 \times 10^{13} \text{ Pa s}$ for the core–mantle boundary layer, a value too low to be compatible with our current understanding of mantle rheology. In this study, therefore, the average viscosity of the core–mantle boundary layer, which is used to calculate the core heat flux using the local stability criterion, is calculated as:

$$\eta = \eta_0 \exp(E/(R(T_L + 0.5(T_{cm} - T_L)) - E/(RT_0))),$$

where η_0 is the reference lower mantle viscosity defined at the lower mantle reference temperature T_0 , E is the activation energy, T_L is the temperature at the top of the boundary layer, T_{cm} is the temperature at the top of the core and R is the universal gas constant. The lower mantle reference temperature T_0 ($\approx 2,763 \text{ K}$) is determined from the reference potential temperature of 1,573 K, and η_0 and E are set to 10^{23} Pa s and 500 kJ mol^{-1} , respectively, based on the estimates of radial viscosity structure of Earth and experimental constraints on activation energy^{59,60}.

For the influence of mantle plumes on melt production, we assume that only a quarter of the temperature contrast at the core–mantle boundary region contributes to upwelling plumes (that is, $f = 0.25$ in equation (24) of ref. 15; see also refs. 61,62). Unlike ref. 15, we do not suppress plume magmatism in the early phase of thermal evolution, but melt production below 10 GPa is always disregarded because melt is expected to be denser than the surrounding mantle at those pressures⁶³.

Given the likelihood of the Rayleigh–Taylor instability associated with the basalt–eclogite transition, crustal growth is limited to the thickness of 30 km (refs. 55,64). After the thickness reaches this limit, the addition of new crustal materials owing to mantle melting is compensated by the recycling of existing crustal materials to the mantle to maintain the same crustal thickness. Furthermore, new crustal materials are divided into the extrusive and intrusive parts, and only the extrusive part is assumed to degas volatiles, including water and argon, to the atmosphere. Volatiles contained in the intrusive part can be recycled back to the mantle with crustal recycling. Based on the structure of Earth's oceanic crust, we assume that the extrusive part constitutes 10% of every new crustal material. In a previous model¹⁵, all melt was assumed to contribute to surface magmatism, thereby overestimating the contribution of mantle melting to atmospheric argon. For radiogenic heating, we use the following abundances: U = 16 ppb, Th/U = 4 ppb and K/U = 7,000 ppb. We performed a sensitivity test and found that our model results are valid for crustal thicknesses up to 60 km, and extrusion rates up to 20%.

The influence of a late-accretion impact is taken into account by modelling the evolution of the radial thermal profile within the core, in the framework of the parameterized convection of model¹⁵. At the chosen time of a hypothetical impact event, the azimuthally averaged temperature increase within the core, with respect to the pre-impact core thermal state, is first calculated from a relevant SPH simulation result. This temperature increase taken from the SPH simulation is added to the core adiabat in the parameterized convection model at one time step before, and this new core thermal profile is then subject to the mantle-side temperature of the core–mantle boundary (Supplementary Fig. 5). The subsequent evolution of the core temperature is modelled with a time increment of 10^3 years (that is, three orders of magnitude shorter than the increment used for the long-term thermal evolution) with radial thermal conduction. At every time step, the corresponding potential temperature is calculated, and the effect of convective mixing is taken into account by resetting the temperature of a superadiabatic region to its average adiabatic temperature (Supplementary Fig. 5). Every 10^6 years, the mantle-side temperature of the core–mantle boundary is revised according to the thermal evolution of the rest of the mantle. As the thermal evolution of the mantle is affected by the core heat flux, which depends on the core temperature, this coupled modelling approach assures the self-consistent evaluation of the influence of a superheated core on the long-term evolution of the mantle. By azimuthally averaging the core temperature, we are assessing the impact of a superheated core in a conservative manner. The broad hottest region seen in Fig. 3a has temperatures around 7,000 K, which would probably have resulted in more intense mantle plume activities than predicted by our one-dimensional (1D) model, but such hotter-than-average regions would cool faster because of higher-than-average regional core heat flow, thereby approaching to

the azimuthally averaged situation. Exploring three-dimensional (3D) effects is thus important for the details of very early plume magmatism, although such details may not concern this work given that the surface of Venus is geologically young. We also note that comparison between 1D and 3D modelling has been done for Mars, and the 1D modelling has been shown to be adequate for broad trends⁶⁵.

The surface temperature is set to 730 K, which reflects the considerable greenhouse effect of the CO₂-rich, dense Venusian atmosphere. We neglect the effect of the time-dependent atmospheric composition for three reasons. First, the primary accretion phase of a terrestrial planet is energetic enough to create a deep magma ocean, and because CO₂ is much less soluble than H₂O (ref. 66), the primordial atmosphere after magma ocean solidification should already be as CO₂-rich as the present-day Venusian atmosphere. By contrast, H₂O in a magma ocean is likely to be trapped in a solidifying magma ocean owing to the rheological transition and the Rayleigh–Taylor instability^{14,67}. Second, the likely evolution of atmospheric composition would result in the variation of surface temperature by ~200 K (for instance, refs. 68,69), which would hardly affect the magnitude of magmatism in the mode of stagnant lid convection. Third, ref. 11 showed that impact-driven atmospheric loss was insignificant. Ref. 11 modelled the influence of a thermal anomaly by the partial melting of the mantle, arriving at the conclusion that an impact would enhance volatile degassing. However, the energetic late-accretion events discussed in this work would create a shallow magma ocean (Fig. 1), and because of the magma solubilities of CO₂ and H₂O as mentioned above, they would hardly affect the atmospheric composition. Without the efficient sequestration of atmospheric carbon by plate tectonics¹⁴, most carbon should already exist in the atmosphere before late accretion, so late accretion would not result in enhanced degassing of CO₂. We note that the consideration of the likely consequences of magma ocean solidification has been absent in previous studies on the thermal evolution of terrestrial planets (for example, see the review paper of ref. 70).

The purpose of our convection modelling is to assess the first-order influence of early energetic impacts on long-term mantle dynamics; therefore, the use of parameterized convection is deemed sufficient. Our model takes into account mantle melting, the secular evolution of mantle viscosity due to cooling as well as dehydration, extrusive versus intrusive magmatism and crustal delamination, and all of these are important to relate mantle dynamics to observables such as atmospheric argon, surface age and crustal thickness. Various other complications that have been suggested for mantle convection in Earth or Venus are considered to be of secondary nature. For example, the possibility of layered convection for a hotter mantle (for example, ref. 71) is not considered because it requires a strongly negative Clapeyron slope for the breakdown of ringwoodite to bridgmanite and ferropericlase, and existing experimental constraints do not support such a negative Clapeyron slope (for example, refs. 72–74). Compositional effects other than the time-varying concentration of water and heat-producing elements are also neglected. Compositional effects associated with lithological heterogeneities may be important for the long-term evolution of Earth's mantle (for example, ref. 75), because plate tectonics keeps differentiating the mantle by magmatism and returning differentiated products (that is, oceanic crust and depleted lithospheric mantle) to the mantle by subduction. In stagnant lid convection, such two-way mass transport does not take place, and even in intermittent plate tectonics (which is difficult to justify from the rheology perspective), the extent of two-way mass transport is limited. We note that our parameterization of mantle melting is thermodynamically more consistent with the current understanding of igneous petrology than those adopted in previous two-dimensional and 3D simulation studies^{9,76,77}.

Our parameterized convection model is based on the continuous operation of stagnant lid convection throughout the history of Venus. We assume that a water ocean never formed on Venus, which

is a high-likelihood scenario if we consider the effect of magma ocean solidification on long-term planetary evolution⁶⁷. Although the possibility of an ocean and even plate tectonics for early Venus continues to be discussed in the literature (for example, refs. 78,79), the continuous operation of stagnant lid convection under a dense CO₂-rich atmosphere remains a valid, self-consistent scenario, which can naturally arise from the solidification of a magma ocean at the end of the primary accretion of Venus. Furthermore, high surface temperatures created by large late-accretion impacts could drastically enhance hydrogen escape⁸⁰, preventing the late formation of a water ocean. Finally, we note that a recently proposed mode of mantle convection, 'plutonic-squishy lid'⁸¹, is based on depth-independent yield strength, that is, a non-trivial cohesive strength and a negligible friction coefficient, which is inconsistent with our understanding of rock mechanics⁸². The subduction of lithosphere on a local scale by mantle plumes^{83,84} is a possibility, but it also depends on the particular assumptions of mantle rheology, which warrant further investigation.

Venus's highly siderophile elements

Highly siderophile elements (HSEs)⁸⁵ have been used to constrain the total mass accreted by Earth after the closure of their core (similar data are available for Mars, the Moon and Vesta). At present, there are no data for Venus crustal or mantle concentrations of HSEs, but it is interesting to consider what the consequences of the high-velocity impacts might be for the retention of HSEs. Here we track the fate of projectile HSEs following the analysis in refs. 6,7, which assumes the projectile's HSEs are confined in their cores. We find that high-velocity late-accretion impacts (25 km s⁻¹, 30 km s⁻¹) are capable of delivering concentrations of HSEs to the bulk silicate Venus that are similar to those delivered to bulk silicate Earth by average impacts (19 km s⁻¹; Supplementary Fig. 9). Thus, a prediction of our model is that Venus's rocks should have HSE abundances similar to those of terrestrial rocks, provided that the initially delivered HSEs are retained in the bulk silicate Venus as on Earth.

Data availability

All data are available in the paper, figures or Supplementary Information. Inputs for numerical simulations are described in the text, and available from the corresponding author upon request.

References

1. Nesvorný, D., Roig, F. V. & Deienno, R. The role of early giant-planet instability in terrestrial planet formation. *AJ* **161**, 50 (2021).
2. Izidoro, A. et al. Planetesimal rings as the cause of the Solar System's planetary architecture. *Nat. Astron.* **6**, 357–366 (2022).
3. Emsenhuber, A., Asphaug, E., Cambioni, S., Gabriel, T. S. & Schwartz, S. R. Collision chains among the terrestrial planets. II. An asymmetry between Earth and Venus. *Planet. Sci. J.* **2**, 199 (2021).
4. Bottke, W. F., Walker, R. J., Day, J. M. D., Nesvorný, D. & Elkins-Tanton, L. Stochastic late accretion to Earth, the Moon, and Mars. *Science* **330**, 1527–1530 (2010).
5. Marchi, S. et al. Widespread mixing and burial of Earth's Hadean crust by asteroid impacts. *Nature* **511**, 578–582 (2014).
6. Marchi, S., Canup, R. M. & Walker, R. J. Heterogeneous delivery of silicate and metal to the Earth by large planetesimals. *Nat. Geosci.* **11**, 77–81 (2018).
7. Marchi, S., Walker, R. J. & Canup, R. M. A compositionally heterogeneous martian mantle due to late accretion. *Sci. Adv.* **6**, eaay2338 (2020).
8. Gillmann, C. et al. Dry late accretion inferred from Venus's coupled atmosphere and internal evolution. *Nat. Geosci.* **13**, 265–269 (2020).
9. Armann, M. & Tackley, P. J. Simulating the thermochemical magmatic and tectonic evolution of Venus's mantle and lithosphere: two-dimensional models. *J. Geophys. Res.* **117**, E12003 (2012).

10. Nakajima, M. et al. Scaling laws for the geometry of an impact-induced magma ocean. *Earth Planet. Sci. Lett.* **568**, 116983 (2021).
11. Gillmann, C., Golabek, G. J. & Tackley, P. J. Effect of a single large impact on the coupled atmosphere-interior evolution of Venus. *Icarus* **268**, 295–312 (2016).
12. Arkani-Hames, J. & Olson, P. Giant impacts, core stratification, and failure of the Martian dynamo. *J. Geophys. Res.* **115**, E07012 (2010).
13. Miyazaki, Y. & Korenaga, J. On the timescale of magma ocean solidification and its chemical consequences: 2. Compositional differentiation under crystal accumulation and matrix compaction. *J. Geophys. Res. Solid Earth* **124**, 3399–3419 (2019).
14. Miyazaki, Y. & Korenaga, J. A wet heterogeneous mantle creates a habitable world in the Hadean. *Nature* **603**, 86–90 (2022).
15. O'Rourke, J. G. & Korenaga, J. Thermal evolution of Venus with argon degassing. *Icarus* **260**, 128–140 (2015).
16. Schubert, G., Turcotte, D. L., & Olson, P. *Mantle Convection in Earth and Planets* (Cambridge Univ. Press, 2001).
17. Solomatov, V. S. Scaling of temperature- and stress-dependent viscosity convection. *Phys. Fluids* **7**, 266–274 (1995).
18. Kasting, J. F. Runaway and moist greenhouse atmospheres and the evolution of Earth and Venus. *Icarus* **74**, 472–494 (1988).
19. Hamano, K., Abe, Y. & Genda, H. Emergence of two types of terrestrial planet on solidification of magma ocean. *Nature* **497**, 607–610 (2013).
20. Korenaga, J. Plate tectonics and surface environment: role of the oceanic upper mantle. *Earth-Sci. Rev.* **205**, 103185 (2020).
21. Grimm, R. E. & Hess, P. C. in *Venus II: Geology, Geophysics, Atmosphere, and Solar Wind Environment* (eds Bougher, S. W. et al.) 1205–1244 (Univ. Arizona Press, 1997).
22. Herrick, R. R. & Sharpton, V. L. Implications from stereo-derived topography of Venusian impact craters. *J. Geophys. Res.* **105**, 20245–20262 (2000).
23. Romeo, I. & Turcotte, D. L. Resurfacing on Venus. *Planet. Space Sci.* **58**, 1374–1380 (2010).
24. Strom, R., Schaber, G. & Dawson, D. The global resurfacing of Venus. *J. Geophys. Res.* **99**, 10899–10926 (1994).
25. Le Feuvre, M. & Wieczorek, M. Nonuniform cratering of the terrestrial planets. *Icarus* **197**, 291–306 (2008).
26. Bottke, W. F. et al. On asteroid impacts, crater scaling laws, and a proposed younger surface age for Venus. In *47th Lunar and Planetary Science Conference* (2016).
27. Turcotte, D. L. An episodic hypothesis for Venusian tectonics. *J. Geophys. Res.* **98**, 17061–17068 (1993).
28. Moresi, L. & Solomatov, V. Mantle convection with a brittle lithosphere: thoughts on the global tectonic styles of the Earth and Venus. *Geophys. J. Int.* **133**, 669–682 (1998).
29. Reese, C. C., Solomatov, V. S. & Moresi, L.-N. Non-Newtonian stagnant lid convection and magmatic resurfacing on Venus. *Icarus* **139**, 67–88 (1999).
30. Parmentier, E. M. & Hess, P. C. Chemical differentiation of a convecting planetary interior: consequences for a one plate planet such as Venus. *Geophys. Res. Lett.* **19**, 2015–2018 (1992).
31. Smrekar, S. E., Davaille, A. & Sotin, C. Venus interior structure and dynamics. *Space Sci. Rev.* **214**, 88 (2018).
32. Jacobson, S. A., Rubie, D. C., Hernlund, J., Morbidelli, A. & Nakajima, M. Formation, stratification, and mixing of the cores of Earth and Venus. *Earth Planet. Sci. Lett.* **474**, 375–386 (2017).
33. Stevenson, D. J., Spohn, T. & Schubert, G. Magnetism and thermal evolution of the terrestrial planets. *Icarus* **54**, 466–489 (1983).
34. O'Rourke, J. G., Gillmann, C. & Tackley, P. J. Prospects for an ancient dynamo and modern crustal remanent magnetism on Venus. *Earth Planet. Sci. Lett.* **502**, 46–56 (2018).
35. Springel, V. The cosmological simulation code GADGET-2. *Mon. Not. R. Astron. Soc.* **364**, 1105–1134 (2005).
36. Melosh, H. J. A hydrocode equation of state for SiO₂. *Meteorit. Planet. Sci.* **42**, 2079–2098 (2007).
37. Thompson, S. L. *ANEOS Analytic Equations of State for Shock Physics Codes Input Manual*. No. SAND-89-2951 (Sandia National Labs., 1990).
38. Marcus, R. A., Stewart, S. T., Sasselov, D. & Hernquist, L. Collisional stripping and disruption of super-Earths. *Astrophys. J.* **700**, L118 (2009).
39. Marcus, R. A. *The Role of Giant Impacts in Planet Formation and Internal Structure*. PhD thesis, Harvard Univ. (2011).
40. Čuk, M. & Stewart, S. T. Making the Moon from a fast-spinning Earth: a giant impact followed by resonant despinning. *Science* **338**, 1047–1052 (2012).
41. Melosh, H. J. Why the Moon is so like the Earth. *Nat. Geosci.* **12**, 402–403 (2019).
42. Hosono, N., Karato, S. I., Makino, J. & Saitoh, T. R. Terrestrial magma ocean origin of the Moon. *Nat. Geosci.* **12**, 418–423 (2019).
43. Canup, R. M. Simulations of a late lunar-forming impact. *Icarus* **168**, 433–456 (2004).
44. Rufu, R., Aharonson, O. & Perets, H. B. A multiple-impact origin for the Moon. *Nat. Geosci.* **10**, 89–94 (2017).
45. Alemi, A. & Stevenson, D. Why Venus has no moon. In *AAS/Division for Planetary Sciences Meeting Abstracts*, Vol. 38 (2006).
46. Gold, T. & Soter, S. Atmospheric tides and the resonant rotation of Venus. *Icarus* **11**, 356–366 (1969).
47. Laskar, J. & Robutel, P. The chaotic obliquity of the planets. *Nature* **361**, 608–612 (1993).
48. Correia, A. & Laskar, J. The four final rotation states of Venus. *Nature* **411**, 767–770 (2001).
49. Correia, A. C. & Laskar, J. Long-term evolution of the spin of Venus: II. Numerical simulations. *Icarus* **163**, 24–45 (2003).
50. Zahnle, K. J., Lupu, R., Dobrovolskis, A. & Sleep, N. H. The tethered moon. *Earth Planet. Sci. Lett.* **427**, 74–82 (2015).
51. Fuller, J., Luan, J. & Quataert, E. Resonance locking as the source of rapid tidal migration in the Jupiter and Saturn moon systems. *Mon. Not. R. Astron. Soc.* **458**, 3867–3879 (2016).
52. Salmon, J. & Canup, R. M. Lunar accretion from a Roche-interior fluid disk. *Astrophys. J.* **760**, 83 (2012).
53. Hesselbrock, A. J. & Minton, D. A. Three dynamical evolution regimes for coupled ring-satellite systems and implications for the formation of the Uranian Satellite Miranda. *Astron. J.* **157**, 30 (2019).
54. Fraeman, A. A. & Korenaga, J. The influence of mantle melting on the evolution of Mars. *Icarus* **210**, 43–57 (2010).
55. O'Rourke, J. G. & Korenaga, J. Terrestrial planet evolution in the stagnant-lid regime: size effects and the formation of self-destabilizing crust. *Icarus* **221**, 1043–1060 (2012).
56. Davaille, A. & Jaupart, C. Onset of thermal convection in fluids with temperature-dependent viscosity: application to the oceanic mantle. *J. Geophys. Res.* **99**, 19853–19866 (1994).
57. Solomatov, V. S. & Moresi, L.-N. Scaling of time-dependent stagnant lid convection: application to small-scale convection on Earth and other terrestrial planets. *J. Geophys. Res.* **105**, 21795–21817 (2000).
58. Watts, A. B. & Zhong, S. Observations of flexure and the rheology of oceanic lithosphere. *Geophys. J. Int.* **142**, 855–875 (2000).
59. Forte, A. M., Simmons, N. A. & Grand, S. P. in *Treatise on Geophysics* 2nd edn, Vol. 1 (ed. Schubert, G.) 853–907 (Elsevier, 2015).
60. Dobson, D. P., Dohmen, R. & Widenbeck, M. Self-diffusion of oxygen and silicon in MgSiO₃ perovskite. *Earth Planet. Sci. Lett.* **270**, 125–129 (2008).
61. Farnetani, C. G. Excess temperature of mantle plumes: the role of chemical stratification across D". *Geophys. Res. Lett.* **24**, 1583–1586 (1997).

62. Leng, W. & S. Zhong, S. Controls on plume heat flux and plume excess temperature. *J. Geophys. Res.* **113**, B04408 (2008).
63. Stolper, E., Walker, D., Hager, B. H. & Hays, J. F. Melt segregation from partially molten source regions: the importance of melt density and source region size. *J. Geophys. Res.* **86**, 6261–6271 (1981).
64. James, P. B., Zuber, M. T. & Phillips, R. J. Crustal thickness and support of topography on Venus. *J. Geophys. Res. Planets* **118**, 859–875 (2013).
65. Plesa, A.-C., Tosi, N., Grott, M. & Breuer, D. Thermal evolution and Urey ratio of Mars. *J. Geophys. Res. Planets* **120**, 995–1010 (2015).
66. Elkins-Tanton, L. T. Linked magma ocean solidification and atmospheric growth for Earth and Mars. *Earth Planet. Sci. Lett.* **271**, 181–191 (2008).
67. Miyazaki, Y. & Korenaga, J. Inefficient water degassing inhibits ocean formation on rocky planets: an insight from self-consistent mantle degassing models. *Astrobiology* **22**, 713–734 (2022).
68. Phillips, R. J., Bullock, M. A. & Hauck, S. A. Climate and interior coupled evolution of Venus. *Geophys. Res. Lett.* **28**, 1779–1782 (2001).
69. Gillman, C. & Tackley, P. J. Atmosphere/mantle coupling and feedbacks on Venus. *J. Geophys. Res. Planets* **119**, 1189–1217 (2014).
70. Breuer, D. & Moore, W. B. in *Treatise on Geophysics* 2nd edn, Vol. 10 (ed. Schubert, G.) 255–305 (Elsevier, 2015).
71. Wolstencroft, M. & Davies, J. H. Influence of the ringwoodite–perovskite transition on mantle convection in spherical geometry as a function of {Clapeyron} slope and {Rayleigh} number. *Solid Earth* **2**, 315–326 (2011).
72. Hirose, K. Phase transitions in pyrolitic mantle around 670-km depth: implications for upwelling of plumes from the lower mantle. *J. Geophys. Res.* **107**, B2078 (2002).
73. Fei, Y. et al. Experimentally determined postspinel transformation boundary in Mg_2SiO_4 using MgO as an internal pressure standard and its geophysical implications. *J. Geophys. Res.* **109**, B02305 (2004).
74. Ohtani, E. & Litasov, K. D. The effect of water on mantle phase transitions. *Rev. Mineral. Geochem.* **62**, 397–420 (2006).
75. Ballmer, M. D., Schmerr, N. C., Nakagawa, T. & Ritsema, J. Compositional mantle layering revealed by slab stagnation at ~1000-km depth. *Sci. Adv.* **1**, e1500815 (2015).
76. Rolf, T., Steinberger, B., Sruthi, U. & Werner, S. C. Inferences on the mantle viscosity structure and the post-overtake evolutionary state of Venus. *Icarus* **313**, 107–123 (2018).
77. Uppalapati, S., Rolf, T., Crameri, F. & Werner, S. C. Dynamics of lithospheric overturns and implications for Venus's surface. *J. Geophys. Res. Planets* **125**, e06258 (2020).
78. Way, M. J. et al. Was Venus the first habitable world of our solar system? *Geophys. Res. Lett.* **43**, 8376–8383 (2020).
79. Krissansen-Totton, J., Fortney, J. J. & Nimmo, F. Was Venus ever habitable? Constraints from a coupled interior–atmosphere–redox evolution model. *Planet. Sci. J.* **2**, 216 (2021).
80. Modirrousta-Galian, D. & Korenaga, J. The three regimes of atmospheric evaporation for super-Earths and sub-Neptunes. *Astrophys. J.* **943**, 11 (2023).
81. Lourenço, D. L., Rozel, A. B., Ballmer, M. D. & Tackley, P. J. Plutonic-squishy lid: a new global tectonic regime generated by intrusive magmatism on Earth-like planets. *Geochem. Geophys. Geosyst.* **21**, e2019GC008756 (2020).
82. Korenaga, J. On the likelihood of plate tectonics on super-Earths: does size matter? *Astrophys. J.* **725**, L43–L46 (2010).
83. Davaille, A., Smrekar, S. & Tomlinson, S. Experimental and observational evidence for plume-induced subduction on Venus. *Nat. Geosci.* **10**, 349–355 (2017).
84. Gülcher, A. J. P., Gerya, T. V., Montési, L. G. J. & Munch, J. Corona structures driven by plume–lithosphere interactions and evidence for ongoing plume activity on Venus. *Nat. Geosci.* **13**, 547–554 (2020).
85. Walker, R. J. Highly siderophile elements in the Earth, Moon and Mars: update and implications for planetary accretion and differentiation. *Geochemistry* **69**, 101–125 (2009).
86. von Zahn, U., Kumar, S., Niemann, H. & Prinn, R. in *Venus* (eds Hunten, D. M. et al) 299–430 (Univ. Arizona Press, 1983).

Acknowledgements

S.M. acknowledges internal support from the Southwest Research Institute and D. Nesvorný for providing impact velocity files from numerical integrations. R.R. is supported by NASA through a NASA Hubble Fellowship grant no. HST-HF2-51491 awarded by the Space Telescope Science Institute, which is operated by the Association of Universities for Research in Astronomy, Inc., for NASA, under contract NAS5-26555.

Author contributions

S.M. conceived the work and analysed the SPH simulations. R.R. ran the SPH simulations. J.K. ran and analysed the geophysical calculations. All authors contributed to the interpretation of the results and writing of the paper.

Competing interests

The authors declare no competing interests.

Additional information

Supplementary information The online version contains supplementary material available at <https://doi.org/10.1038/s41550-023-02037-2>.

Correspondence and requests for materials should be addressed to Simone Marchi.

Peer review information *Nature Astronomy* thanks the anonymous reviewers for their contribution to the peer review of this work.

Reprints and permissions information is available at www.nature.com/reprints.

Publisher's note Springer Nature remains neutral with regard to jurisdictional claims in published maps and institutional affiliations.

Springer Nature or its licensor (e.g. a society or other partner) holds exclusive rights to this article under a publishing agreement with the author(s) or other rightsholder(s); author self-archiving of the accepted manuscript version of this article is solely governed by the terms of such publishing agreement and applicable law.

© The Author(s), under exclusive licence to Springer Nature Limited 2023